INTERNATIONAL JOURNAL OF
NUMERICAL ANALYSIS AND MODELING
Volume 16, Number 4, Pages 609–625

COUPLING METHOD OF PLANE WAVE DG AND BOUNDARY ELEMENT FOR ELECTROMAGNETIC SCATTERING

QIYA HU, XINGYUE GUO, YANG LIU*, AND HAIJING ZHOU

Abstract. In this paper we are concerned with the coupling of plane wave method and the boundary element method for electromagnetic scattering problems in unbounded domains, which are described by time-harmonic Maxwell's equations. We derive a coupled variational formula of the plane wave discontinuous Galerkin method and the boundary element method for the underlying model problem, and introduce a discretization of the coupled variational problem. The numerical results show that the proposed method is effective.

Key words. Maxwell's equations, plane wave DG method, boundary element method, coupling variational problem.

1. Introduction

Computational electromagnetic has been a hot research field for a long time due to its widely engineering application, such as electromagnetic analysis of circuits, antennas, and wireless communication systems, etc. Differential equations and integral equations are two basic forms for describing engineering problems. Therefore, numerical methods in computational electromagnetic can be classified according to equations they are based on. For example, the finite element method (FEM) and the finite difference time domain (FDTD) are based on differential equations, while method of moments (MoM) and its fast algorithms are based on integral equations. In recent years, with the enhancement of computer technique, many hybrid frameworks of different numerical methods in computational electromagnetic have been developed rapidly for the increasing requirement of more complicated engineering design and optimization.

Time-harmonic Maxwell's equations in unbounded domains is a basic model in the simulation of electromagnetic scattering. There are many methods for the numerical solution of this model problem, and among them the popular one is the coupling of finite element method and the boundary element method (see, for example, [1], [2], [3] and [4]). In recent years, the plane wave methods, which was first proposed for Helmholtz equation (see [5], [6] and [7]), have been extended to the discretization of time-harmonic Maxwell's equations in bounded domains (see [8], [9] and [10]), since the plane wave methods can generate higher accuracy approximations than the other methods for scattering problems with middle or high frequency.

In the present paper, we extend the plane wave method to the discretization of time-harmonic Maxwell's equations in unbounded domains. We first derive a coupled variational formula of the plane wave discontinuous Galerkin (PWDG) method and the boundary element method (BEM) for the electromagnetic scattering problems. Then we introduce a discretization of the coupled variational problem. A solution strategy for the resulting algebraic system is also proposed. In particular, to demonstrate the ability of the proposed method in dealing with complicated problems, we design a strategy for simplify of the coupled variational formula to the case that describes scattering problems of the composite dielectric and conducting objects. We apply the proposed method to simulate several

Received by the editors on June 6, 2017.
2000 *Mathematics Subject Classification.* 65N30, 65N38, 65N55.
∗ Corresponding author.

electromagnetic scattering examples, and we find that the method is effective and can generate approximate solutions with higher accuracy than the coupling of the traditional finite element method and the boundary element method.

The paper is organized as follows: In Section 2, we describe the model problem; We give a variational formulation in bounded domains based on the PWDG method in Section 3; In Section 4, we derive a coupled variational problem of the PWDG method and the boundary element method; The discretization for the coupled variational problem is introduced in Section 5; In section 6, we discuss the application of the proposed method to a particular model describing the scattering problems of the composite dielectric and conducting objects; In Section 7, we report some numerical results; Finally, a conclusion is give in Section 8.

2. Description of underlying Maxwell equations

Let $\Omega \subset \mathbb{R}^3$ be a bounded domain, with Lipschitz-continuous boundary $\Gamma = \partial\Omega$. Set $\Omega^c := \mathbb{R}^3 \backslash \Omega$. The relative permittivity and permeability for the domain Ω are denoted by ϵ_r and μ_r, while ϵ_r^c and μ_r^c are used to present the relative permittivity and permeability for the domain Ω^c. Here, the media in domain Ω^c is assumed to be homogenous dielectric, namely, ϵ_r^c and μ_r^c are constant real numbers. Let ϵ_0 and μ_0 be permittivity and permeability of free space. Then $\kappa_0 := \omega\sqrt{\epsilon_0\mu_0}$ is the wave number of the excitation in free space with $\omega > 0$ being the fixed angular frequency of the excitation. Moreover, the wave number of the excitation in domain Ω and Ω^c are $\hat{\kappa} := \kappa_0\sqrt{\epsilon_r\mu_r}$ and $\kappa := \kappa_0\sqrt{\epsilon_r^c\mu_r^c}$, respectively.

For a vector field $\mathbf{F}$ in Ω or Ω^c, define the traces on Γ by $\gamma_t\mathbf{F} = \mathbf{n} \times (\mathbf{F} \times \mathbf{n})$ and $\gamma_N\mathbf{F} = (\nabla \times \mathbf{F}) \times \mathbf{n}$, where $\mathbf{n}$ denotes the exterior unit normal vector on Γ from Ω into Ω^c.

Let $\mathbf{E}^c$ and $\mathbf{E}$ denote the complex amplitude of the scattered electric field in Ω^c and the total electric field inside Ω, respectively. Consider the transmission problem (cf. [1] and [3])

$$
(1) \qquad \begin{cases}
\nabla \times \nabla \times \mathbf{E}^c - \kappa^2 \mathbf{E}^c = 0 & \text{in} \quad \Omega^c, \\
\nabla \times (\dfrac{1}{\mu_r} \nabla \times \mathbf{E}) - \kappa_0^2 \epsilon_r \mathbf{E} = 0 & \text{in} \quad \Omega, \\
\gamma_t \mathbf{E}^c - \gamma_t \mathbf{E} = -\gamma_t \mathbf{E}_{inc}, \ \dfrac{1}{\mu_r^c} \gamma_N \mathbf{E}^c - \dfrac{1}{\mu_r} \gamma_N \mathbf{E} = -\dfrac{1}{\mu_r^c} \gamma_N \mathbf{E}_{inc} & \text{on} \quad \Gamma, \\
\lim\limits_{|\mathbf{x}| \to \infty} (\nabla \times \mathbf{E} \times \mathbf{x} - i\kappa |\mathbf{x}| \mathbf{E}) = 0,
\end{cases}
$$

where $\mathbf{E}_{inc}$ stands for the complex amplitude of the electric field associated with the incident wave.

We also consider an important variant of the above model. Let Ω be the union of two adjacent subdomains $\Omega^{(1)}$ and $\Omega^{(2)}$, as shown in Figure 1. The electric field $\mathbf{E}$ vanishes on $\Omega^{(2)}$ ($supp$ $\mathbf{E} \subset \Omega^{(1)}$). This particular case describes scattering problems of the composite dielectric and conducting objects, such as micro-strip structures, antenna systems, aircraft or missile with radar radome, etc (refer to [11], [12] and [13]). The subdomain $\Omega^{(1)}$ corresponds to the dielectric region, while the conducting region, in which the electric field $\mathbf{E}$ vanishes, is denoted by the subdomain $\Omega^{(2)}$.

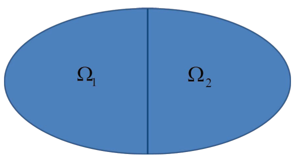

FIGURE 1. The schematic of the two subdomains $\Omega^{(1)}$ and $\Omega^{(2)}$.

Then, we have

(2) $$\gamma_t \mathbf{E} = \mathbf{0} \text{ and } \gamma_t \mathbf{E}^c = -\gamma_t \mathbf{E}_{inc} \text{ on } \Gamma^{(2)} = \Gamma \cap \partial\Omega^{(2)}.$$

Let Ω be divided into a partition in the sense that

$$\overline{\Omega} = \bigcup_{k=1}^{N} \overline{\Omega}_k, \quad \Omega_l \bigcap \Omega_j = \emptyset \quad \text{for } l \neq j.$$

In applications, we require that each element Ω_k is just a tetrahedron, namely, the domain Ω is approximated by a polyhedron Ω_h. Then, without loss of generality, we assume that Ω is just a polyhedron. Let

$$\mathcal{T}_h$$

denote the triangulation comprised of the elements $\{\Omega_k\}$, where h is the meshwidth of the triangulation. Define

$$\Gamma_{lj} = \partial\Omega_l \bigcap \partial\Omega_j, \quad \text{for } l \neq j$$

and

$$\Gamma_k = \overline{\Omega}_k \bigcap \partial\Omega \quad (k = 1, \ldots, N).$$

For each element Ω_k, let $\mathbf{E}|_{\Omega_k} = \mathbf{E}_k$ $(k = 1, \ldots, N)$. Then the second equation in the problem (1) to be solved consists of finding the local electric field $\mathbf{E}_k$ such that

(3) $$\nabla \times (\frac{1}{\mu_r} \nabla \times \mathbf{E}_k) - \kappa_0^2 \epsilon_r \mathbf{E}_k = 0 \qquad \text{in} \quad \Omega_k,$$

with the interface conditions (note that $\mathbf{n}_l = -\mathbf{n}_j$)

(4) $$\begin{cases} \mathbf{n} \times \mathbf{E}_l \times \mathbf{n}_l - \mathbf{n} \times \mathbf{E}_j \times \mathbf{n}_j = 0 \\ (\frac{1}{\mu_r} \nabla \times \mathbf{E}_l) \times \mathbf{n}_l + (\frac{1}{\mu_r} \nabla \times \mathbf{E}_j) \times \mathbf{n}_j = 0 \end{cases} \quad \text{on} \quad \Gamma_{lj} \quad (l < j;\ l, j = 1, 2, \ldots, N).$$

For convenience, we add a fictitious boundary condition on $\partial\Omega$

(5) $$\frac{1}{\mu_r} (\nabla \times \mathbf{E}_l) \times \mathbf{n} = \mathbf{g}, \qquad \text{on} \quad \Gamma_k = \partial\Omega_k \cap \partial\Omega.$$

In the next section we introduce a new variational problem of the Maxwell equations (3), (4), and (5).

3. Plane wave DG method for Maxwell equations in the bounded domain

The plane wave discontinuous Galerkin (PWDG) method for the discretization of time-harmonic Maxwell's equations in bounded domains was proposed in [8]. In this section we give PWDG variational formula of (3), (4), and (5).

For an element Ω_k, let $\mathbf{H}(\text{curl};\ \Omega_k)$ denote the standard Sobolev space, and set

(6) $$\mathbf{V}(\Omega_k) = \Big\{ \mathbf{E}_k \in \mathbf{H}(\text{curl}, \Omega_k);\ \mathbf{E}_k \text{ satisfies the equations (3)} \Big\}.$$

Define

$$\mathbf{V}(\mathcal{T}_h) = \prod_{k=1}^{N} \mathbf{V}(\Omega_k),$$

with the natural L^2-inner product $(\cdot, \cdot)_{\mathbf{V}}$.

For $\mathbf{F} \in \mathbf{V}(\mathcal{T}_h)$, set $\mathbf{F}|_{\Omega_k} = \mathbf{F}_k$. For each local interface Γ_{lj} $(l < j)$, we define the jumps and the averages on Γ_{lj} as follows (note that $\mathbf{n}_l = -\mathbf{n}_j$):

(7) $$\begin{aligned} [\![\mathbf{F}]\!] &= \mathbf{F}_l \times \mathbf{n}_l + \mathbf{F}_j \times \mathbf{n}_j \\ \{\{\mathbf{F}\}\} &= \frac{1}{2} (\mathbf{F}_l + \mathbf{F}_j). \end{aligned}$$

For ease of notation, define

$$\Phi(\mathbf{F_k}) = \frac{1}{\mu_r}(\nabla \times \mathbf{F_k}) \text{ on } \Omega_k.$$

Let α and β be two positive numbers, and let $\delta \in (0, \frac{1}{2}]$. Define the sesquilinear form $\mathcal{A}_h(\cdot,\cdot)$ by

$$\begin{aligned}\mathcal{A}_h(\mathbf{E},\mathbf{F}) = &\sum_{k=1}^{N}\Big(\int_{\Gamma_k}(\mathbf{n}\times\mathbf{E}_k)\cdot\overline{\Phi(\mathbf{F}_k)}ds - \delta\int_{\Gamma_k}\Phi(\mathbf{E}_k)\cdot\overline{\mathbf{n}\times\mathbf{F}_k}ds \\ &- i\kappa_0^{-1}\delta\int_{\Gamma_k}[\mathbf{n}\times\Phi(\mathbf{E}_k)]\cdot[\overline{\mathbf{n}\times\Phi(\mathbf{F}_k)}]ds\Big) \\ &+\sum_{l<j}\Big(\int_{\Gamma_{lj}}\{\{\mathbf{E}\}\}\cdot\overline{[\![\Phi(\mathbf{F})]\!]}ds + \int_{\Gamma_{lj}}\{\{\Phi(\mathbf{E})\}\}\cdot\overline{[\![\mathbf{F}]\!]}ds \\ &- i\kappa_0\alpha\int_{\Gamma_{lj}}[\![\mathbf{E}]\!]\cdot\overline{[\![\mathbf{F}]\!]}\,ds - i\kappa_0^{-1}\beta\int_{\Gamma_{lj}}[\![\Phi(\mathbf{E})]\!]\cdot\overline{[\![\Phi(\mathbf{F})]\!]}\,ds\Big),\ \forall\,\mathbf{F}\in\mathbf{V}(\mathcal{T}_h),\end{aligned} \tag{8}$$

and the functional $\mathcal{L}_h(\cdot,\cdot)$ by

$$\mathcal{L}_h(\mathbf{g},\mathbf{F}) = \sum_{k=1}^{N}\Big(\frac{\delta}{i\kappa_0}\int_{\Gamma_k}(\mathbf{n}_k\times\mathbf{g})\cdot\overline{\Phi(\mathbf{F}_k)}ds + (1-\delta)\int_{\Gamma_k}(\mathbf{n}_k\times\mathbf{g})\cdot\overline{\mathbf{n}_k\times\mathbf{F}_k}ds\Big),\ \forall\mathbf{F}\in\mathbf{V}(\mathcal{T}_h). \tag{9}$$

Then, for a given $\mathbf{g}$, the variational problem associated with (3)-(5) can be expressed as follows: Find $\mathbf{E}\in\mathbf{V}(\mathcal{T}_h)$ such that

$$\mathcal{A}_h(\mathbf{E},\mathbf{F}) = \mathcal{L}_h(\mathbf{g},\mathbf{F}),\ \forall\mathbf{F}\in\mathbf{V}(\mathcal{T}_h). \tag{10}$$

4. Coupled variational formula of the transmission problem

In this section we first derive a boundary integral equation of the field $\mathbf{E}^c$ on the outer domain Ω^c as in [1], then we give a coupled variational formula for the electromagnetic scattering problem.

Let us recall an integral representation of the field $\mathbf{E}^c$ on the unbounded domain Ω^c. As usual, the fundamental solution $G(\mathbf{x},\mathbf{y})$ of the Helmholtz operator $-\Delta - \kappa^2\mathbf{I}$, satisfying the Sommerfeld radiation condition, is given by

$$G(\mathbf{x},\mathbf{y}) = \frac{e^{i\kappa|\mathbf{x}-\mathbf{y}|}}{4\pi|\mathbf{x}-\mathbf{y}|}.$$

Let S and $\mathbf{S}$ denote the scalar (rep. vectorial) single layer potential, mapping any sufficiently smooth function (rep. tangent field) ϕ (rep. $\boldsymbol{\mu}$) on Γ to the field in $\mathbb{R}^3$ defined away from Γ by

$$(S\phi)(\mathbf{x}) = \int_\Gamma G(\mathbf{x},\mathbf{y})\phi(\mathbf{y})ds(\mathbf{y}) \tag{11}$$

and

$$(\mathbf{S}\boldsymbol{\mu})(\mathbf{x}) = \int_\Gamma G(\mathbf{x},\mathbf{y})\boldsymbol{\mu}(\mathbf{y})ds(\mathbf{y}), \tag{12}$$

respectively. They are joined by the Maxwell double layer potential

$$(\mathbf{D}\mathbf{v})(\mathbf{x}) = (\nabla\times\mathcal{S}(\mathbf{n}\times\mathbf{v}))(\mathbf{x}), \tag{13}$$

where $\mathbf{v}$ is a vector field defined in $\mathbb{R}^3$. Define the Maxwell single layer potential for a vector field $\boldsymbol{\mu}$

$$(\mathbf{K}\boldsymbol{\mu})(\mathbf{x}) = (\mathbf{S}\boldsymbol{\mu})(\mathbf{x}) + \frac{1}{\kappa^2}\nabla(S(div_\Gamma\boldsymbol{\mu}))(\mathbf{x}). \tag{14}$$

Then the field $\mathbf{E}^c$ can be expressed as [1]

$$\mathbf{E}^c = \mathbf{D}(\gamma_t\mathbf{E}^c) - \mathbf{K}(\gamma_N\mathbf{E}^c), \text{ in } \Omega^c. \tag{15}$$

Now we can define the coupled variational problem according to (10) and (15), together with the transmission conditions.

For convenience, let γ_t^+ and γ_t^- denote the restriction of the mapping γ_t on vector fields defined in Ω^c and Ω, respectively. Similarly, let γ_N^+ and γ_N^- denote the restriction of the mapping γ_N on vector fields defined in Ω^c and Ω, respectively.

It follows by (15) that

$$\gamma_t^+\mathbf{E}^c = \gamma_t^+\mathbf{D}(\gamma_t^+\mathbf{E}^c) - \gamma_t^+\mathbf{K}(\gamma_N^+\mathbf{E}^c). \tag{16}$$

By the jump relation [14, 3], we have

$$\gamma_t^+\mathbf{D}(\gamma_t^+\mathbf{E}^c) = \gamma_t^-\mathbf{D}(\gamma_t^+\mathbf{E}^c) + \gamma_t^+\mathbf{E}^c \text{ and } \gamma_t^+\mathbf{K}(\gamma_N^+\mathbf{E}^c) = \gamma_t^-\mathbf{K}(\gamma_N^+\mathbf{E}^c).$$

Substituting these into (16), together with the first interface condition, yields

$$\gamma_t^+\mathbf{E}^c = \gamma_t^-\mathbf{D}(\gamma_t^-\mathbf{E} - \gamma_t\mathbf{E}_{inc}) + \gamma_t^+\mathbf{E}^c - \gamma_t^-\mathbf{K}(\gamma_N^+\mathbf{E}^c).$$

Namely,

$$\gamma_t^-\mathbf{D}(\gamma_t^-\mathbf{E}) - \gamma_t^-\mathbf{K}(\gamma_N^+\mathbf{E}^c) = \gamma_t^-\mathbf{D}(\gamma_t\mathbf{E}_{inc}) \text{ on } \Gamma. \tag{17}$$

On the other hand, the field $\mathbf{g}$ in $\mathcal{L}_h(\mathbf{g},\mathbf{F})$ is just $\gamma_N^-\mathbf{E}$. Then, by the second interface condition, the equation (10) can be written in the form

$$\mathcal{A}_h(\mathbf{E},\mathbf{F}) = \frac{1}{\mu_r^c}\mathcal{L}_h(\gamma_N^+\mathbf{E}^c + \gamma_N\mathbf{E}_{inc},\mathbf{F}), \ \forall\mathbf{F} \in \mathbf{V}(\mathcal{T}_h).$$

Set $\gamma_N^+\mathbf{E}^c = \boldsymbol{\lambda}$. By the above equation and (17), leads to

$$\mathcal{A}_h(\mathbf{E},\mathbf{F}) = \frac{1}{\mu_r^c}\mathcal{L}_h(\boldsymbol{\lambda},\mathbf{F}) + \frac{1}{\mu_r^c}\mathcal{L}_h(\gamma_N\mathbf{E}_{inc},\mathbf{F}), \ \forall\mathbf{F} \in \mathbf{V}(\mathcal{T}_h) \tag{18}$$

and

$$\langle\gamma_t^-\mathbf{D}(\gamma_t^-\mathbf{E}),\boldsymbol{\mu}\rangle_\Gamma - \langle\gamma_t^-\mathbf{K}(\boldsymbol{\lambda}),\boldsymbol{\mu}\rangle_\Gamma = \langle\gamma_t^-\mathbf{D}(\gamma_t\mathbf{E}_{inc}),\boldsymbol{\mu}\rangle_\Gamma, \ \forall\boldsymbol{\mu} \in H_{div}^{-\frac{1}{2}}(\Gamma). \tag{19}$$

Notice that $\boldsymbol{\mu}$ can be written as $\boldsymbol{\mu} = \mathbf{v}\times\mathbf{n}$ for $\mathbf{v} \in \mathrm{H}(\mathbf{curl},\Omega)$, the mapping γ_t^- in the front of the operators $\mathbf{D}$ and $\mathbf{K}$ is unnecessary. Moreover, we have

$$\mathbf{n}\times\gamma_t^-\mathbf{E} = \mathbf{n}\times\mathbf{E}.$$

Therefore, we can define the sesquilinear forms $\mathcal{B}_h(\cdot,\cdot)$ and $C_h(\cdot,\cdot)$ by

$$\mathcal{B}_h(\mathbf{E},\boldsymbol{\mu}) = \langle\gamma_t^-\mathbf{D}(\gamma_t^-\mathbf{E}),\boldsymbol{\mu}\rangle_\Gamma = \int_\Gamma\int_\Gamma(\nabla_\mathbf{x}G(\mathbf{x},\mathbf{y})\times(\mathbf{n}\times\mathbf{E})(\mathbf{y}))\cdot\boldsymbol{\mu}(\mathbf{x})ds(\mathbf{y})ds(\mathbf{x})$$

and

$$\begin{aligned} C_h(\boldsymbol{\lambda},\boldsymbol{\mu}) &= \langle\gamma_t^-\mathbf{K}(\boldsymbol{\lambda}),\boldsymbol{\mu}\rangle_\Gamma = \int_\Gamma\int_\Gamma G(\mathbf{x},\mathbf{y})\boldsymbol{\lambda}(\mathbf{y})\cdot\boldsymbol{\mu}(\mathbf{x})ds(\mathbf{y})ds(\mathbf{x}) \\ &- \frac{1}{\kappa^2}\int_\Gamma\int_\Gamma G(\mathbf{x},\mathbf{y})div_\Gamma\boldsymbol{\lambda}(\mathbf{y})div_\Gamma\boldsymbol{\mu}(\mathbf{x})ds(\mathbf{y})ds(\mathbf{x}). \end{aligned}$$

Similarly, define

$$\mathcal{D}_h(\gamma_t\mathbf{E}_{inc},\boldsymbol{\mu}) = \langle\gamma_t^-\mathbf{D}(\gamma_t\mathbf{E}_{inc}),\boldsymbol{\mu}\rangle_\Gamma = \int_\Gamma\int_\Gamma(\nabla_\mathbf{x}G(\mathbf{x},\mathbf{y})\times(\mathbf{n}\times\mathbf{E}_{inc})(\mathbf{y}))\cdot\boldsymbol{\mu}(\mathbf{x})ds(\mathbf{y})ds(\mathbf{x}).$$

From (18) and (19), we obtain the coupled variational problem: to find $\mathbf{E} \in V(\mathcal{T}_h)$ and $\boldsymbol{\lambda} \in H_{div}^{-\frac{1}{2}}(\Gamma)$ such that

$$\mathcal{A}_h(\mathbf{E},\mathbf{F}) - \frac{1}{\mu_r^c}\mathcal{L}_h(\boldsymbol{\lambda},\mathbf{F}) = \frac{1}{\mu_r^c}\mathcal{L}_h(\gamma_N\mathbf{E}_{inc},\mathbf{F}), \ \forall\mathbf{F} \in \mathbf{V}(\mathcal{T}_h) \tag{20}$$

and

$$\mathcal{B}_h(\mathbf{E},\boldsymbol{\mu}) - C_h(\boldsymbol{\lambda},\boldsymbol{\mu}) = \mathcal{D}_h(\gamma_t\mathbf{E}_{inc},\boldsymbol{\mu}),\ \forall\boldsymbol{\mu}\in H_{div}^{-\frac{1}{2}}(\Gamma). \tag{21}$$

We would like to point out that the formula (21) is *simpler* than the one derived in [1].

5. Discretization for the coupled variational problem

In this section, we introduce a discretization of the coupled variational problem (21).

5.1. The plane wave basis functions. In this subsection we construct a finite-dimensional space $\mathbf{V}_p(\mathcal{T}_h)\subset\mathbf{V}(\mathcal{T}_h)$. We first give the precise definition of such a space $\mathbf{V}_p(\mathcal{T}_h)$.

In practice, following Ref. [10], a suitable family of plane waves, which are solutions of the constant-coefficient Maxwell equations, are generated on Ω_k by choosing p unit propagation directions $\mathbf{d}_l$, $l=1,\dots,p$ (we use the optimal spherical codes from [15]) and defining a real unit polarization vector $\mathbf{G}_l$ orthogonal to $\mathbf{d}_l$. Then the propagation directions and polarization vectors define the complex polarization vectors $\mathbf{F}_l$ and $\mathbf{F}_{l+p}$ by

$$\mathbf{F}_l = \mathbf{G}_l + \mathrm{i}\mathbf{G}_l\times\mathbf{d}_l,\quad \mathbf{F}_{l+p} = \mathbf{G}_l - \mathrm{i}\mathbf{G}_l\times\mathbf{d}_l\ (l=1,\dots,p).$$

Note that the complex polarization vectors are the same as in Refs. [16, 10], but differ slightly from those in Ref. [8]. We then define the complex functions $\mathbf{E}_l$:

$$\mathbf{E}_l = \sqrt{\mu_r}\,\mathbf{F}_l\exp(\mathrm{i}\hat{\kappa}\mathbf{d}_l^*\cdot\mathbf{x})\ (l=1,\dots,2p), \tag{22}$$

where $\mathbf{d}_l^* = d_l$ for $l=1,\cdots,p$ and $\mathbf{d}_l^* = d_{l-p}$ when $l=p+1,\cdots,2p$. It is easy to verify that every function $\mathbf{E}_l$ $(l=1,\dots,2p)$ satisfies Maxwell's system (3).

Let Q_{2p} denote the space spanned by the $2p$ plane-wave functions $\mathbf{E}_l$ $(l=1,\dots,2p)$. Define the finite-element space

$$\mathbf{V}_p(\mathcal{T}_h) = \Big\{\mathbf{v}\in L^2(\Omega):\ \mathbf{v}|_K\in Q_{2p}\text{ for any }K\in\mathcal{T}_h\Big\}. \tag{23}$$

It is easy to see that the above space has $N\times 2p$ basis functions, which are defined by

$$\phi_l^k(\mathbf{x}) = \begin{cases}\mathbf{E}_l(\mathbf{x}),\ \mathbf{x}\in\Omega_k,\\[2ex] 0,\ \mathbf{x}\in\Omega_j\text{ satisfying }j\neq k\end{cases}\qquad (k=1,\dots,N;\ l=1,\dots,2p). \tag{24}$$

5.2. The basis functions in the boundary element space. The triangulation $\mathcal{T}_h$ on Ω generate natural mesh nodes on Γ. By using such mesh nodes on Γ, we obtain a triangulation $\mathcal{T}_h^\Gamma$ on Γ_h which approximates Γ (Γ_h is just the boundary of the polyhedron Ω_h). Let $W_h(\mathcal{T}_h^\Gamma)\subset H_{div}^{-\frac{1}{2}}(\Gamma_h)$ denote the two-dimensional Raviart-Thomas finite element space [17] on the surface mesh. For this finite element space, there is one vectorial basis function associated with each edge (there are three vectorial basis functions on each triangle element). In the following, we define the basis functions of $W_h(\mathcal{T}_h^\Gamma)$. Since $\boldsymbol{\mu}\in H_{div}^{-\frac{1}{2}}(\Gamma_h)$ can be written as $\boldsymbol{\mu}=\mathbf{v}\times\mathbf{n}$ with $\mathbf{v}\in \mathrm{H}(\mathbf{curl},\Omega)$, we can define the basis functions of $W_h(\mathcal{T}_h^\Gamma)$ by edge finite element basis functions on the triangulation $\mathcal{T}_h$.

Let e_{lj} be an edge of $\mathcal{T}_h^\Gamma$, whose two endpoints are denoted by V_l and V_j, and let T be an triangle containing e_{lj} as one of its edges. Besides, let K be a tetrahedron containing T as one of its face. We use λ_i and λ_j, which are linear polynomials on K, to denote the nodal basis function at the two endpoints V_l and V_j, respectively. Then the desired basis function on the edge e_{ij} can be written as

$$L_{ij} = (\lambda_l\nabla\lambda_j - \lambda_j\nabla\lambda_l)\times\mathbf{n}_T\text{ on }T,$$

where $\mathbf{n}_T$ denote the outer unit normal vector of T. It is known that

$$div_\Gamma L_{ij} = (\nabla\times(\lambda_l\nabla\lambda_j - \lambda_j\nabla\lambda_l))\cdot\mathbf{n}_T\text{ on }T.$$

Let T' satisfying $e_{ij} \subset T' \subset \Gamma_h$ denote the neighboring element with T. We similarly define L_{ij} on T'. Notice that L_{ij} may take different values on T and T'. We naturally extend L_{ij} to global Γ_h by zero, and define

$$W_h(\mathcal{T}_h^{\Gamma}) = spann\{L_{ij}\}.$$

5.3. Discrete variational formula of the coupled problem. Let $\mathbf{V}_p(\mathcal{T}_h)$ and $W_h(\mathcal{T}_h^{\Gamma})$ be defined as in the previous subsections. The discrete variational problem associated with the equations (20) and (21) can be described as follows: To find $\mathbf{E}_h \in \mathbf{V}_p(\mathcal{T}_h)$ and $\boldsymbol{\lambda}_h \in W_h(\mathcal{T}_h^{\Gamma})$ such that

$$\begin{cases} \mathcal{A}_h(\mathbf{E}_h, \mathbf{F}_h) - \dfrac{1}{\mu_r^c}\mathcal{L}_h(\boldsymbol{\lambda}_h, \mathbf{F}_h) = \dfrac{1}{\mu_r^c}\mathcal{L}_h(\gamma_N \mathbf{E}_{inc}, \mathbf{F}_h), \ \forall \mathbf{F}_h \in \mathbf{V}_p(\mathcal{T}_h) \\ \mathcal{B}_h(Q_h\mathbf{E}_h, \boldsymbol{\mu}_h) - C_h(\boldsymbol{\lambda}_h, \boldsymbol{\mu}_h) = \mathcal{D}_h(\gamma_t \mathbf{E}_{inc}, \boldsymbol{\mu}_h), \ \forall \boldsymbol{\mu}_h \in W_h(\mathcal{T}_h^{\Gamma}). \end{cases} \tag{25}$$

In applications, we can consider three choices of the parameters α, β and δ: (1) $\alpha = \beta = \delta = \frac{1}{2}$; (2) $\alpha = 2$ and $\beta = \delta = \frac{1}{3}$; (3) $\alpha = \frac{p}{h\kappa_0 \log(p)}$ and $\beta = \delta = \frac{h\kappa_0 \log(p)}{p}$.

With the finite dimensional spaces $\mathbf{V}_p(\mathcal{T}_h)$ and $W_h(\mathcal{T}_h^{\Gamma})$, let A, B, C and L denote the matrices associated with the sesquilinear forms $\mathcal{A}_h(\cdot,\cdot)$, $\mathcal{B}_h(\cdot,\cdot)$, $C_h(\cdot,\cdot)$ and $-\mathcal{L}_h(\cdot,\cdot)$, respectively. The equations (25) can be written into the algebraic form

$$\begin{pmatrix} A & L \\ B & C \end{pmatrix} \begin{pmatrix} \chi \\ y \end{pmatrix} = \begin{pmatrix} \xi \\ b \end{pmatrix}. \tag{26}$$

It is expensive to solve the above system in the direct manner.

Eliminating the unknown χ from (26), we get

$$(C - BA^{-1}L)y = b - BA^{-1}\xi. \tag{27}$$

We observed that the condition number of the Schur complement matrix $K = C - BA^{-1}L$ is much smaller than that of the plane wave stiffness matrix A. In Subsection 7.1, we list the condition numbers of the matrices A and K for the considered example to illustrate this conclusion. This conclusion can be intuitively understood: the operator corresponding to K is defined on a lower order Sobolev space (trace space) than the one corresponding to A (refer to [1] and [8]). However, it seems a bit complicated to theoretically prove this conclusion for the current situation. Based on this observation, we can solve the system (27) by GMRES method, where the action of A^{-1} is implemented by preconditioned GMRES method with a preconditioner $\hat{A}$ of A, and the actions of B and C are implemented by the fast multipole method [11]. An effective preconditioner $\hat{A}$ was constructed in [9].

6. An important variant of the equation (1)

In this section, we discuss the variant mentioned in Section 2 for scattering problems of the composite dielectric and conducting objects. Many numerical methods have been discussed for simulating this kind of scattering problems due to its wide application demands, among which the popular methods are the MoM of volume-surface integral equations [11], the coupling of finite element method and the boundary element method [12], and hybrid of several methods based on domain decomposition methods [13]. For this case, we can derive a simpler formula from the proposed coupling of plane wave DG method and the boundary element method.

As described in Section 2, for this case Ω is the union of two subdomains $\Omega^{(1)}$ and $\Omega^{(2)}$, and $\mathbf{E}$ vanishes on $\Omega^{(2)}$ ($supp\ \mathbf{E} \subset \Omega^{(1)}$). Then

$$\gamma_t\mathbf{E} = \mathbf{0} \text{ on } \Gamma^{12} = \partial\Omega^{(1)} \cap \partial\Omega^{(2)} \text{ and } \gamma_t\mathbf{E}^c = -\gamma_t\mathbf{E}_{inc} \text{ on } \Gamma^{(2)} = \Gamma \cap \partial\Omega^{(2)}. \tag{28}$$

Besides, there exists an interface field $\mathbf{J}_s \in H_{div}^{-\frac{1}{2}}(\partial\Omega^{(2)})$ such that

(29)
$$\gamma_N \mathbf{E} = \mathbf{J}_s \text{ on } \Gamma^{12} = \partial\Omega^{(1)} \cap \partial\Omega^{(2)} \text{ and } \frac{1}{\mu_r^c}\gamma_N \mathbf{E}^c - \frac{1}{\mu_r}\mathbf{J}_s = -\frac{1}{\mu_r^c}\gamma_N \mathbf{E}_{inc} \text{ on } \Gamma^{(2)} = \Gamma \cap \partial\Omega^{(2)}.$$

We can regard the first condition in (28) as the Dirichelet boundary condition of $\mathbf{E}$ on Γ_{12}. Then we can first compute E on $\Omega^{(1)}$ by the FEM-BEM coupling method on $\Omega^{(1)} \cup \Omega^c$.

By (3.3) in [8], we have for each element K

$$\int_{\partial K} \mathbf{n} \times \hat{\mathbf{E}}_{h,p} \cdot \overline{\mu_r^{-1}\nabla \times \xi_{h,p}} ds + i\kappa_0 \int_{\partial K} \mathbf{n} \times \hat{H}_{h,p} \cdot \overline{\xi_{h,p}} ds = 0. \tag{30}$$

Recall the numerical fluxes as functions on the interior face F

$$\hat{\mathbf{E}}_{h,p} = \{\{\mathbf{E}_{h,p}\}\} + \frac{\beta}{i\kappa_0}[\![\mu^{-1}\nabla \times \mathbf{E}_{h,p}]\!],$$

$$\hat{\mathbf{H}}_{h,p} = \frac{1}{i\kappa_0}[\![\mu_r^{-1}\nabla \times \mathbf{E}_{h,p}]\!] - \alpha[\![\mathbf{E}_{h,p}]\!].$$

In addition, we define new numerical fluxes on Γ^{12}

$$\hat{\mathbf{E}}_{h,p} = \mathbf{E}_{h,p} - \delta(\mathbf{n} \times \mathbf{E}_{h,p}) \times \mathbf{n},$$

$$\hat{\mathbf{H}}_{h,p} = \frac{1}{i\kappa_0\mu_r}\nabla \times \mathbf{E}_{h,p} + \sqrt{\frac{\epsilon_r}{\mu_r}}(1-\delta)(\mathbf{n} \times \mathbf{E}_{h,p}),$$

and on $\Gamma^{(1)} = \Gamma \cap \partial\Omega^{(1)}$

$$\hat{\mathbf{E}}_{h,p} = \mathbf{E}_{h,p} - \delta(\frac{1}{i\kappa_0}\mathbf{n} \times (\mu_r^{-1}\nabla \times \mathbf{E}_{h,p}) + \frac{1}{i\kappa_0}\mathbf{g}),$$

$$\hat{\mathbf{H}}_{h,p} = \frac{1}{i\kappa_0\mu_r}\nabla \times \mathbf{E}_{h,p} - (1-\delta)(\frac{1}{i\kappa_0\mu_r}\nabla \times \mathbf{E}_{h,p} - \frac{1}{i\kappa_0}\mathbf{n} \times \mathbf{g}).$$

It is easy to see that we have on $\Gamma^{(12)}$

$$\mathbf{n} \times \hat{\mathbf{E}}_{h,p} = (1-\delta)\mathbf{n} \times \mathbf{E}_{h,p} \text{ and } \mathbf{n} \times \hat{\mathbf{H}}_{h,p} = \frac{1}{i\kappa_0}\mathbf{n} \times \Phi(\mathbf{E}_{h,p}) + \sqrt{\frac{\epsilon_r}{\mu_r}}(1-\delta)\mathbf{n} \times (\mathbf{n} \times \mathbf{E}_{h,p}).$$

Define

$$\Gamma_k^{(1)} = \Gamma^{(1)} \cap \partial\Omega_k,\ \Gamma_k^{(12)} = \Gamma^{(12)} \cap \partial\Omega_k$$

and

$$\Gamma_{kj}^{(1)} = \partial\Omega_k \cap \partial\Omega_j,\ \text{for } \Omega_k, \Omega_j \subset \Omega^{(1)}.$$

Substituting the numerical fluxes into (30), and summing it over all the elements, yields

$$\mathcal{A}_h^{(1)}(\mathbf{E}_h, \mathbf{F}_h) + \mathcal{A}_h^{(12)}(\mathbf{E}_h, \mathbf{F}_h) = \mathcal{L}_h^{(1)}(\mathbf{g}, \mathbf{F}_h), \tag{31}$$

where $\mathcal{A}_h^{(1)}(\cdot,\cdot)$ is obtained by changing Γ_k into $\Gamma_k^{(1)}$ and Γ_{kj} into $\Gamma_{kj}^{(1)}$ in $\mathcal{A}_h(\cdot,\cdot)$, and $\mathcal{L}_h^{(1)}(\mathbf{g},\cdot)$ is obtained by changing Γ_k into $\Gamma_k^{(1)}$ in $\mathcal{L}_h(\mathbf{g},\cdot)$ and $\mathcal{A}_h^{(12)}(\cdot,\cdot)$ is defined by

$$\mathcal{A}_h^{(12)}(\mathbf{E}_h, \mathbf{F}_h) = (1-\delta)\int_{\Gamma_k^{(12)}} (\mathbf{n} \times \mathbf{E}_h) \cdot \overline{\Phi(\mathbf{F}_h)} + \int_{\Gamma^{(12)}} (\mathbf{n} \times \Phi(\mathbf{E}_h)) \cdot \overline{\mathbf{F}}_h ds$$
$$- i\kappa_0(1-\delta)\int_{\Gamma^{(12)}} (\mathbf{n} \times \mathbf{E}_h) \cdot \overline{\mathbf{n} \times \mathbf{F}_h} ds.$$

After getting $\nabla \times E^c$ on $\Gamma^{(1)}$ and $\mathbf{E}_h$ on $\Omega^{(1)}$ by (31) and the boundary integral equation on $\Gamma^{(1)}$, we can compute $\mathbf{J}_s$ on $\Gamma^{(12)}$ by the first equality in (29). The fields $\nabla \times E^c$ and $\mathbf{J}_s$ on $\Gamma^{(2)}$ can be computed by the second equality in (29) and the boundary integral equation on $\Gamma^{(2)}$. In the following, we would like to explain this in details.

Define

$$\mathcal{B}_h^{(1)}(\mathbf{E}_h,\boldsymbol{\mu}_h)=\int_{\Gamma}\left(\int_{\Gamma^{(1)}}(\nabla_{\mathbf{x}}G(\mathbf{x},\mathbf{y})\times\mathbf{Q}_h^{(1)}(\mathbf{n}\times\mathbf{E}_h)(\mathbf{y}))ds(\mathbf{y})\right)\cdot\boldsymbol{\mu}_h(\mathbf{x})ds(\mathbf{x}),$$

where $\mathbf{Q}_h^{(1)}:(V_p(\mathcal{T}_h)\times\mathbf{n})|_{\Gamma_h^{(1)}}\to W_h(\mathcal{T}_h^{\Gamma^{(1)}})$ denotes L^2 projector. Set $\mathbf{E}_h^{(1)}=\mathbf{E}_h|_{\Omega^{(1)}}$ and $V_p(\mathcal{T}_h^{(1)})=V_p(\mathcal{T}_h)|_{\Omega^{(1)}}$. Then, by (31) and the second equality in (25), we obtain the coupling variational problem: find $\mathbf{E}_h^{(1)}\in\mathbf{V}_p(\mathcal{T}_h^{(1)})$ and $\boldsymbol{\lambda}_h\in W_h(\mathcal{T}_h^{\Gamma})$ such that

$$(32)\quad\begin{cases}\tilde{\mathcal{A}}_h^{(1)}(\mathbf{E}_h^{(1)},\mathbf{F}_h)-\dfrac{1}{\mu_r^c}\mathcal{L}_h^{(1)}(\boldsymbol{\lambda}_h,\mathbf{F}_h)=\dfrac{1}{\mu_r^c}\mathcal{L}_h^{(1)}(\gamma_N\mathbf{E}_{inc},\mathbf{F}_h),\ \forall\mathbf{F}_h\in\mathbf{V}_p(\mathcal{T}_h^{(1)})\\[2mm] \mathcal{B}_h^{(1)}(\mathbf{E}_h^{(1)},\boldsymbol{\mu}_h)-C_h(\boldsymbol{\lambda}_h,\boldsymbol{\mu}_h)=\mathcal{D}_h(\gamma_t\mathbf{E}_{inc},\boldsymbol{\mu}_h),\ \forall\boldsymbol{\mu}_h\in W_h(\mathcal{T}_h^{\Gamma}),\end{cases}$$

where

$$\tilde{\mathcal{A}}_h^{(1)}(\mathbf{E}_h^{(1)},\mathbf{F}_h)=\mathcal{A}_h^{(1)}(\mathbf{E}_h,\mathbf{F}_h)+\mathcal{A}_h^{(12)}(\mathbf{E}_h,\mathbf{F}_h).$$

For the considered particular case, there is no variable or triangulation in the interior of subdomain $\Omega^{(2)}$. We only take the equivalent surface electric current on the surface of subdomain $\Omega^{(2)}$ as the variable and triangulation for the subdomain $\Omega^{(2)}$ is only given on the surface of $\Omega^{(2)}$.

We would like to point out that the proposed method can be applied to more general situations that we do not assume $supp\ \mathbf{E}\subset\Omega^{(1)}$. Of course, for more general situations we can not derive such a simple formula as in this section. For the general situation, the subdomain $\Omega^{(1)}$ is discretized by tetrahedrons and the resulting triangulation in the subdomain $\Omega^{(1)}$ generates natural mesh nodes on the interface of the two subdomains. By using these mesh nodes on the interface, we obtain a conformal surface triangulation on subdomain $\Omega^{(2)}$.

7. Numerical experiments

In this section, some numerical examples are presented to demonstrate the accuracy and convergence performance of the proposed coupling of plane wave DG method and the boundary element method. All examples are considered in free space and the method of moments (MoM) is adopted to obtain the reference results. The error of near (far) field is measured in the L^2-norm, defined as

$$(33)\qquad \text{error}=\sqrt{\frac{\sum_{j=1}^{N}\left|\mathbf{E_{num,j}}-\mathbf{E_{MoM,j}}\right|^2}{\sum_{j=1}^{N}\left|\mathbf{E_{MoM,j}}\right|^2}},$$

where $\mathbf{E_{num,j}}$ denotes the numerical results of near (far) field with PWDG-BEM, and $\mathbf{E_{MoM,j}}$ denotes the corresponding numerical results of near (far) field with MoM.

7.1. The scattering problem of a dielectric cube. In the first example, we investigate the accuracy and convergence performance of the proposed method by simulating the scattering problem of a dielectric cube, as shown in Figure 2. An incident x-polarized plane wave is from the z direction onto the dielectric cube, which has the edge length of 0.4 m. The wavelength λ of the plane wave in free space is 1 m. The relative permittivity ϵ_r and permeability μ_r for the dielectric cube are 1.3 and 1.0, respectively.

Firstly, we use the proposed PWDG-BEM and traditional FEM-BEM to get the bistatic radar cross section (RCS) with different mesh sizes in Figure 3. In the PWDG-BEM, the parameter p for generating a family of plane waves is chosen as 25 and the mesh sizes

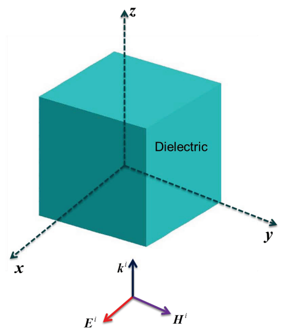

FIGURE 2. The schematic of a dielectric cube scattering.

are $\lambda_d/3$, $\lambda_d/4$ and $\lambda_d/5$, respectively. On the other hand, the mesh sizes for FEM-BEM are $\lambda_d/5$, $\lambda_d/16$, $\lambda_d/18$ and $\lambda_d/20$, respectively, where λ_d is the wavelength of the incident wave in the dielectric object. From the Figures 3(a) and 3(b), it can be seen that both methods get better accuracy with denser mesh. However, to reach a certain accuracy, the number of unknowns used by PWDG-BEM is less than that of FEM-BEM, which is displayed in Table 1. The advantage of PWDG-BEM will become more obvious for large scale problems.

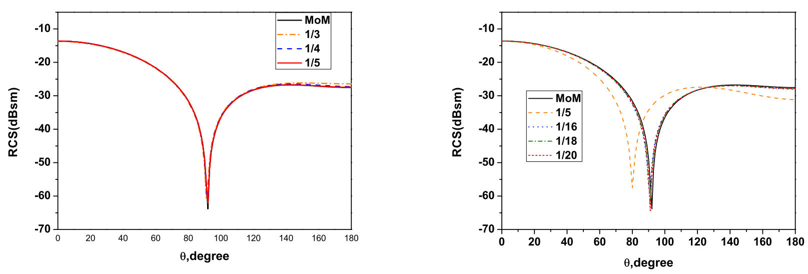

(a) PWDG-BEM (b) FEM-BEM

FIGURE 3. Bistatic RCS given by PWDG-BEM and FEM-BEM with d-ifferent mesh sizes.

TABLE 1. Triangulations for PWDG-BEM adn FEM-BEM.

Method	Mesh Size	Tetrahedrons	Edges on Surface	Unknowns
PWDG-BEM	$\lambda_d/5$	128	123	$128 \times 25 \times 2 + 123 = 6523$
FEM-BEM	$\lambda_d/20$	8056	1941	10503

There are three choices of parameter α, β and δ, whose formulations are given in section 5.3. To explore effects of these parameters on the accuracy of PWDG-BEM, we investigate the error of near (far) field, defined in (33), with different number of unknowns. It is noted that the number of unknowns depends on both the mesh size and the number of propagation of directions. Therefore, we first fix the mesh size at $\lambda_d/5$, the errors of RCS and near field are demonstrated in Figure (4) with respect to the number of propagation

TABLE 2. The number of unknowns for PWDG-BEM and time cost with respect to p.

The parameter p	9	16	25	36	49	64	81
The number of unknowns	2427	4219	6523	9339	12667	16507	20859
Time cost (Type 1)	43.48	59.97	106.73	229.63	504.56	1084.61	2191.78
Time cost (Type 2)	43.29	59.63	106.44	223.35	493.84	1063.52	2140.95
Time cost (Type 3)	43.8	61.07	107.89	224.89	496.88	1073.12	2169.23

directions, respectively. Moreover, the corresponding number of unknowns and time cost are displayed in Table 2, where "Type i ($i = 1, 2, 3$)" means to adopt different type of parameters α, β and δ.

Figure 4(a) shows that the error of near field does not depend on the type of parameters α, β and δ when p is large than 16. It can also be seen from Figure 4(b) that the type of parameters α, β and δ has few influence on the RCS error when p is between 16 and 49. However, the RCS error is better with the third type of parameters α, β and δ when p is larger than 49.

Then we consider the errors of RCS and far field with respect to the mesh size for the fixed number of propagation of directions p. Since the type of parameters α, β and δ makes little difference on the accuracy of PWDG-BEM when p is large than 16, we only use the the first type of parameters. Table 3 presents the number of unknowns with different mesh size. Figure 5 displays the variety of near field (RCS) error with respect to the parameter h, which is the number of meshes in each wavelength, for $p = 16$ or 25. It is illuminated that the mesh size impacts the error of near field (RCS) slightly in Figure 5 (a). In addition, the parameter p dominates the effect on the accuracy of PWDG-BEM compared with the mesh size. The time cost is also displayed with respect to the parameter h in Figure 5 (b).

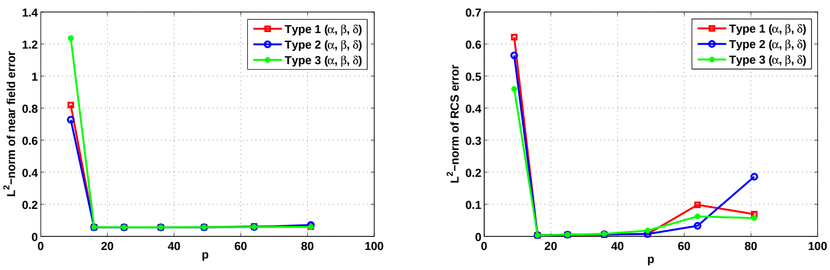

(a) Near field error (b) RCS error

FIGURE 4. The errors of near field and RCS with respect to p.

In addition, we employ the PWDG-BEM to get the distribution of electric field magnitude. Figure 6 presents the distribution of electric field magnitude in xoy plane given by PWDG-BEM with $p = 25$ and mesh size being $\lambda_d/9$. For demonstrating the effects of mesh size on the distribution of electric field, we also give total and each components of electric field magnitude along x axis with different mesh sizes in Figure 7. Figure 8 gives the errors of far field and near field with respect to the wave number. For each wave number, the mesh size is fixed at $\lambda/5$. It can be seen that the errors of far and near fields of this example vary slightly, which means the stability of the proposed method with respect

TABLE 3. The number of unknowns for PWDG-BEM.

mesh size	$\lambda_d/3$	$\lambda_d/4$	$\lambda_d/5$	$\lambda_d/6$	$\lambda_d/7$
The number of tetrahedrons	24	58	128	198	352
The number of unknowns ($p = 16$)	804	1928	4219	6492	11501
The number of unknowns ($p = 25$)	1236	2972	6523	10056	17837

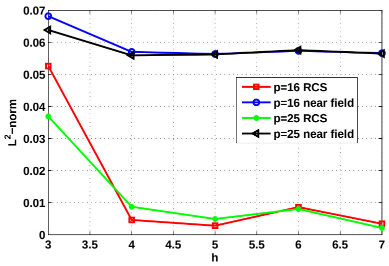

(a) Near field and RCS error

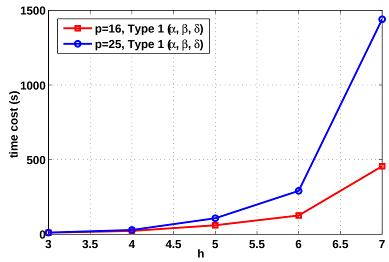

(b) Time cost

FIGURE 5. The errors of near field and RCS with respect to the mesh size and time cost.

to the wave number. All numerical results of PWDG-BEM are compared with those of MoM.

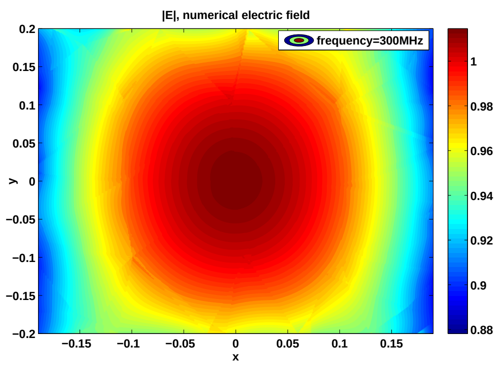

FIGURE 6. The schematic of a dielectric cube scattering.

In order to illustrate stability of the proposed method, we increase the wave number κ but fix the mesh size $h = \lambda_d/5$ and the direction number $p = 16$. In Figure 8, we show the L^2 norms of the errors of the resulting approximations.

This figure indicates that the accuracy of the near field almost has no wave number pollution but the accuracy of the far field slightly becomes worse when increasing the wave number. Of course, we can either decrease the mesh size h or increase the direction number p to keep the high accuracy of the far field.

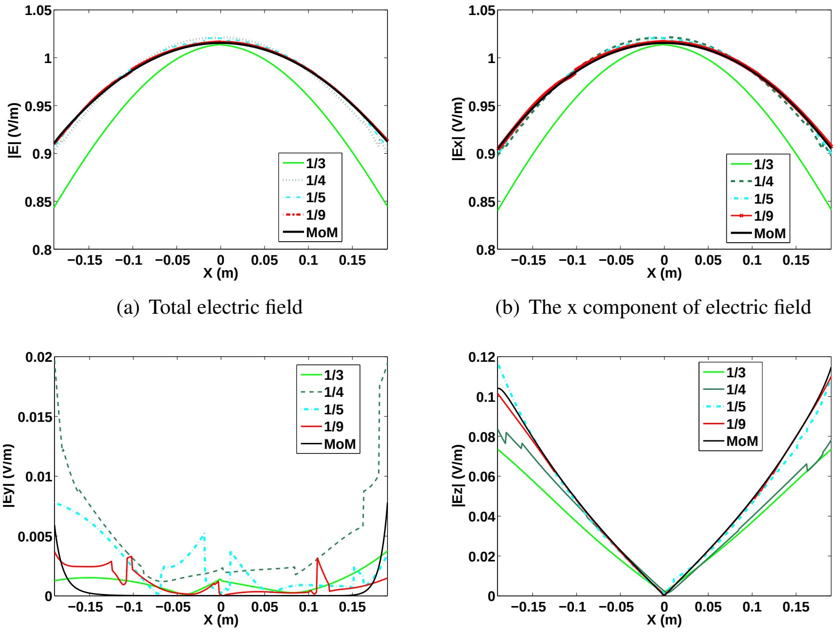

(a) Total electric field

(b) The x component of electric field

(c) The y component of electric field

(d) The z component of electric field

FIGURE 7. The total and each components of electric field magnitude with different mesh size.

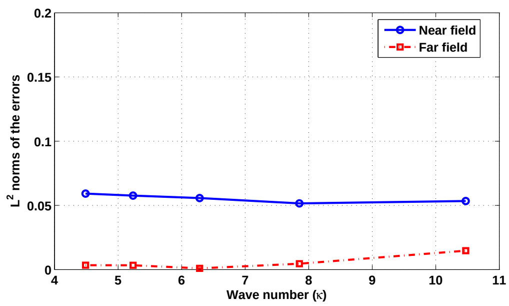

FIGURE 8. The L^2 norms of the errors of near field and far field with respect to the wave numbers.

We would like to compare the condition numbers of the plane wave stiffness matrix A and the Schur complement matrix K defined at the bottom of Section 5. We list the data in Table 4.

It can be seen from Table 4 that the condition number of the matrix K is indeed much smaller than that of the matrix A.

7.2. The scattering problem of a dielectric-PEC conjunct object. To illuminate the validity of PWDG-BEM for solving the particular case discussed in section 6, we consider the scattering problem of a dielectric-PEC conjunct object in Figure 9. The conjunct object contains a dielectric cylinder with relative permittivity ϵ_r and permeability μ_r and a perfect

TABLE 4. Condition numbers of the matrices A and K with respect to wave number κ.

Wave Length (m)	1.4	1.2	1.0	0.8	0.6
Wave number	4.49	5.24	6.28	7.85	10.47
Condition number of the matrix A	1.24e7	2.47e7	2.49e9	2.71e8	1.49e8
Condition number of the matrix K	18.92	27.96	23.24	31.38	1.56e2

electric conductor (PEC) hemisphere. The radius and height of the cylinder are 0.15 m and 0.2 m, while the radius of hemisphere is 0.15 m. The conjunct object is also excited by an x-polarized plane wave incident from z direction, whose wavelength is 1 m. We use the PWDG-BEM to obtain the bistatic RCS for different ϵ_r (ϵ_r = 1.5 and ϵ_r = 2.0) in Figure 10. It is demonstrated that the numerical results of PWDG-BEM agree well with those of MoM.

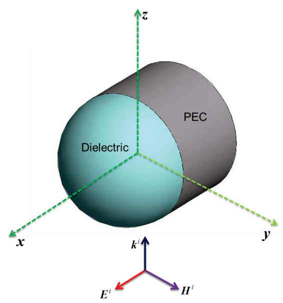

FIGURE 9. The schematic of a dielectric-PEC conjunct object.

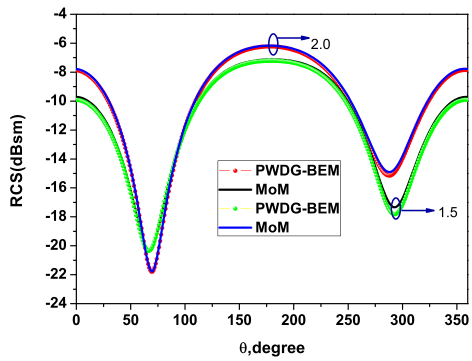

FIGURE 10. Bistatic RCS of the conjunct object with different ϵ_r given by PWDG-BEM.

7.3. The scattering problem of a PEC aircraft with dielectric nose. For displaying the advantage of the preconditioner mentioned in subsection 5.3, the preconditioned PWDG-BEM is adopted to analyze the scattering problem of a PEC aircraft with dielectric nose in Figure 11. The relative permittivity of the dielectric nose, $\epsilon_r = 1.3$ and the size of the aircraft is $14\ m \times 2.4\ m \times 0.7\ m$. The incident z-polarized plane wave is from x direction and its frequency is 40 MHz. We first use the PWDG-BEM to get the bistatic RCS of the scattering problem in polar coordinate, as shown in Figure 12. Here, the parameter p is 16 and the triangulation has 1968 triangles and 168 tetrahedrons in the dielectric part. By comparison with the numerical result of MoM, we can see that the PWDG-BEM has good accuracy. Since the iteration solvers, such as GMRES method, can not converge to a given tolerance in dealing with the problem, the LU factorization method is used. It shows that the bad condition number of PWDG-BEM limits its application for large scale problems.

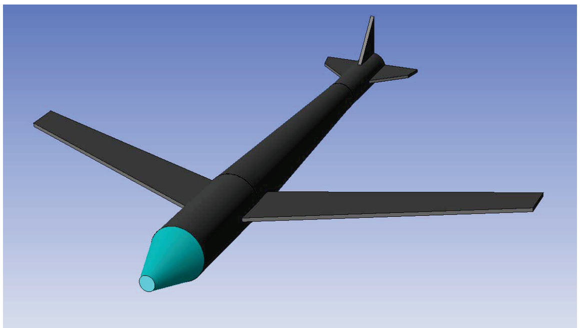

FIGURE 11. The schematic of a PEC aircraft with dielectric nose.

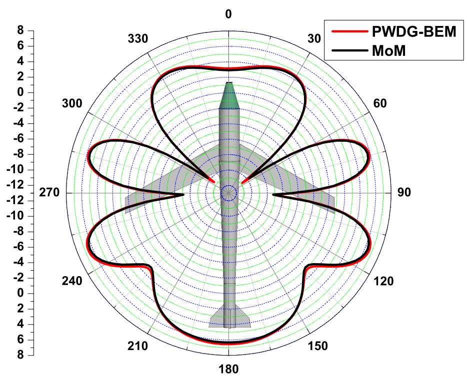

FIGURE 12. The bistatic RCS in polar coordinate with PWDG-BEM.

To improve the condition number, we construct the preconditioner for PWDG-BEM by partitioning the dielectric nose into 12 parts, as shown in Figure 13. The preconditioned PWDG-BEM can converge to the tolerance $1.0e-4$ with 272 iteration steps for solving the problem and its validity is illuminated in Figure 14. It also reveals the potential capability of preconditoned PWDG-BEM in analyzing the large scale problems.

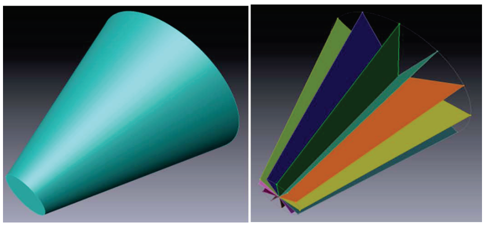

FIGURE 13. The partition of the dielectric nose.

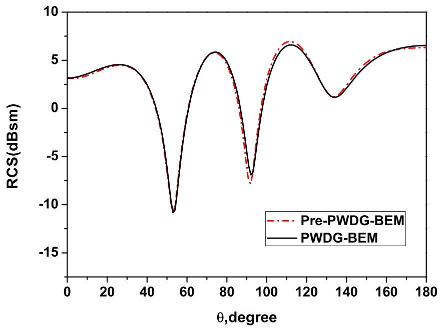

FIGURE 14. The bistatic RCS with preconditioned PWDG-BEM.

8. Conclusion

A coupling of plane wave DG method and the boundary element method for electromagnetic scattering problems in unbounded domains is presented in this paper. We derive a coupled variational formula of the PWDG-BEM, and introduce a discretization of the coupled variational problem. In particular, we give the variational formula in detail to the case that describes scattering problems of the composite dielectric and conducting objects. Some numerical results demonstrate the effectiveness and accuracy of the proposed method. Compared with the coupling of traditional finite element method and the boundary element method, the proposed PWDG-BEM can provide a higher accurate solution.

Acknowledgments

The research was supported in part by the National Natural Science Foundation of China (Grant No. 11571352, 11571196, 61201113), the Science Challenge Program (Grant No. JCKY2016212A502), the Science Technology Foundation of China Academy of Engineering Physics (Grant No. 2015B0403094), Major State Basic Research Development Program of China (Grant No. 2013CB328900), National Natural Science Foundation of China (Grant No. 61431014) and the Key Project of Complicated Electromagnetic Environment Laboratory, CAEP (Grant No.2015E01−1).

References

[1] R. Hiptmair, Coupling of finite elements and boundary elements in electromagnetic scattering, SIAM J. Numer. Anal., 41(3) (2003) 919-944.

[2] C. Johnson, J. Nedelec, On the coupling of boundary integral and finite element methods, Math. Comput., 35(1980) 1063-1079.

[3] J. C. Nédélec, Acoustic and Electromagnetic Equations: Integral Representations for Harmonic Problems, Applied Mathematical Sciences, New York: Springer, Berlin, 2001.

[4] F. J. Sayas, The validity of Johnson-Nedéléc's BEM-FEM coupling on polygonal interfaces, SIAM J. Numer. Anal., 47(5) (2009) 3451-3463.
[5] O. Cessenat and B. Despres, Application of an ultra weak variational formulation of elliptic pdes to the two-dimensional helmholtz problem, SIAM J. Numer. Anal. 35(1) (1998) 255-299.
[6] C. Farhat, R. Tezaur and J. Toivanen, A domain decomposition method for discontinuous Galerkin discretizations of Helmholtz problems with plane waves and Lagrange multipliers, Int. J. Numer. Meth. Engng. 78 (2009) 1513-1531.
[7] R. Hiptmair, A. Moiola and I. Perugia, Plane wave discontinuous Galerkin methods for the 2D Helmholtz equation: analysis of the p-version, SIAM J. Numer. Anal., 49 (2011) 264-284.
[8] R. Hiptmair, A. Moiola, and I. Perugia, Error analysis of Trefftz-discontinuous Galerkin methods for the time-harmonic Maxwell equations, Math. Comp., 82 (281) (2013) 247-268.
[9] Q. Hu and L. Yuan, A plane-wave least-squares method for time-harmonic Maxwell's equations in absorbing media, SIAM J. Sci. Comput., 36 (4) (2014) 1937-1959.
[10] T. Huttunen, M. Malinen, P. Monk, Solving Maxwell's equations using the ultra weak variational formulation, J. Comput. Phys., 223 (2) (2007) 731-758.
[11] W. C. Chew, J. M. Jin, E. Midielssen, J. M. Song, Fast and efficient algorithms in computational electromagnetics, MA: Artech House, Boston, 2001.
[12] J. M. Jin, The finite element method in electromagnetics, John Wiley & Sons, New York, 2002.
[13] X. Wang, Z. Peng, M. Stephanson and J. F. Lee, Modeling EMC/EMI effects of antenna systems on large platforms using multi-solver domain decomposition methods, The 4th European Conference on Antennas and Propagation, Barcelona, Spain, April 2010.
[14] D. Colton and R. Kress, Integral equation methods in scattering theory, FL: Krieger Publication, Melbourne, 1983.
[15] N. Sloane, Tables of spherical codes, http://www2.research.att.com/njas/packings, 2000.
[16] O. Cessenat and B. Despres, Using plane waves as basis functions for solving time harmonic equations with the ultra weak variational formulation, J. Comput. Acous., 11 (2) (2003) 227-238.
[17] P. Raviart and J. Thomas, A Mixed Finite Element Method for Second Order Elliptic Problems, Lecture Notes in Mathematics, vol. 606, Berlin, New York: Springer, 1977.

1. LSEC, ICMSEC, Academy of Mathematics and Systems Science, Chinese Academy of Sciences, Beijing 100190, China; 2. School of Mathematical Sciences, University of Chinese Academy of Sciences, Beijing 100049, China
E-mail: hqy@lsec.cc.ac.cn

the School of Electronics Engineering and Computer Science, Peking University, Beijing 100871, China.
E-mail: gxy4010@126.com

Institute of Applied Physics and Computational Mathematics, Beijing 100094, China.
E-mail: liu_yang@iapcm.ac.cn and zhou_haijing@iapcm.ac.cn